Simulation of self-assembled compositional core-shell structures in In_{x}Ga_{1−x}N nanowires

Xiaobin Niu, Gerald B. Stringfellow, Young-Ju Lee, and Feng Liu

Phys. Rev. B **85**, 165316 — Published 20 April 2012

DOI: 10.1103/PhysRevB.85.165316

Simulation of self-assembled compositional core-shell structures in InGaN nanowires

Xiaobin Niu,[1] Gerald B. Stringfellow,[1,2] Young-Ju Lee,[3] Feng Liu[1,*]

[1]*Department of Materials Sciences and Engineering, University of Utah, Salt Lake City, Utah 84112, USA*

[2]*Department of Electrical and Computer Engineering, University of Utah, Salt Lake City, Utah 84112, USA*

[3]*Department of Mathematics, Rutgers, The State University of New Jersey, New Jersey 08854, USA*

ABSTRACT

We report the simulation of compositional core-shell structure formation in epitaxial InGaN nanowires (NWs) and its dependence on kinetic growth mode and epitaxial relation to substrate, based on atomistic-strain-model Monte Carlo simulations. On a lattice mismatched substrate, the layer-by-layer growth results in self-assembled core-shell structures with the core rich in the unstrained component (relative to the substrate), while the faceted growth mode leads to the strained core component, and both are distinctively different from the equilibrium composition profiles. Our simulation results explain the reason that all the existing core-shell alloy NWs grown by vapor-liquid-solid experiments have cores rich in the unstrained (or less strained) components is because they have been grown via the layer-by-layer mode, and more importantly suggest a possible route towards controlling the NW core-shell composition by altering growth mode and/or selecting substrate.

PACS numbers: 68.35.Dv, 68.65.La, 81.05.Ea, 81.07.Vb, 81.16.Dn

* Corresponding author, fliu@eng.utah.edu

I. INTRODUCTION

Formation of heterostructures and junctions in alloy nanowires (NWs) during epitaxial growth processes is a key strategy for producing optimal nanophotonic and nanoelectronic materials, including high efficiency blue and green light-emitting diodes (LEDs)[1,2], visible lasers[3,4] and high efficiency solar cells[5]. Desirable device functions may be realized by the formation of axial (superlattice)[6] or radial (core-shell) heterostructures in NWs[7], as their electronic and optical properties are in part determined by their composition profiles (CPs). A number of methods have been used to fabricate core-shell NWs. One approach is to specifically grow the cores and shells in two steps by changing growth conditions to vary the growth mechanism. Often, the cores are first formed using the vapor-liquid-solid (VLS) mechanism, followed by the growth of shells on the sides of the cores using higher temperatures or different reactants during epitaxial growth[7,8]. However, this approach faces challenges for cost-effective device fabrication, because it is time consuming and the conditions are sometimes difficult to control. An alternative desirable strategy would be the spontaneous formation of self-assembled core-shell structures[9-12], which has also seen great success in self-assembled alloy thin films[13,14] and quantum dots[15,16].

Alloy NWs are experimentally observed to either have uniform CPs[17,18] or phase separated to core-shell structure[9,10]. Those NWs with uniform CPs are usually grown at low temperature and high growth rate, which limit surface diffusion and thus suppress the tendency toward phase separation. The spontaneously formed core-shell NWs are experimentally observed to most often accumulate the strained components in the shell[9-12]. (Here, strain of a component is defined by its lattice mismatch to substrate.) Good control of the CPs in the self-assembled NWs is lacking partly because the physical mechanism underlying the self-assembly is unclear. The reason for such uncertainty is mainly because these structures are usually grown under non-equilibrium conditions. If thermodynamic equilibrium were achieved throughout the NW, no core-shell structure would be observed. In reality, however, the alloy CPs in NWs are expected to be distinctly different from the equilibrium distribution, because bulk diffusion with an energy barrier of a few eVs[19] is negligible at typical growth temperatures. On the other

hand, local equilibrium is often established in the near surface region due to the more rapid surface (and sub-surface) diffusion with a much smaller energy barrier in the order of 1 eV[20] or smaller. Consequently, the growth mode is expected to be a key factor in determining the kinetically limited CPs in NWs, similar to the case of self-assembled alloy quantum dots[15,16].

In this work, we report the simulation of compositional core-shell structure formation in epitaxial InGaN NWs and its relation to the kinetic growth mode and substrate. We have performed atomistic-strain-model Monte Carlo (MC) simulations[21] of the VLS growth of strained NWs by considering two different growth modes: layer-by-layer growth (LG) versus faceted growth (FG). Our calculations show that LG produces core-shell structures with the core rich in the unstrained (or less strained) component; while FG produces structures with the core rich in the strained component. These growth-mode-controlled alloy CPs are shown to be distinctly different from the equilibrium profiles.

II. SIMULATION METHOD

The spontaneous core-shell formation during the growth of InGaN NWs is simulated by minimizing the Gibbs free energy, $G = H - TS$ using the atomistic-strain-model Monte Carlo MC method, where $H = \Omega x_A x_B = E_{\mathrm{el}} + E_{\mathrm{s}}$ is the enthalpy and S is the configuration entropy of mixing of the system. The total elastic strain energy E_{el} is calculated using an atomistic strain model[22,23], which assumes harmonic potentials and includes nearest-neighbor (NN), next-NN (NNN), and bond-bending (BB) interactions (Fig. 1). $E_{el} = k_n\left(S_{xx}^2 + S_{yy}^2\right) + k_{nn}\left[\left(S_{xx} + 2S_{xy} + S_{yy}\right)^2 + \left(S_{xx} - 2S_{xy} + S_{yy}\right)^2\right] + k_{bb}S_{xy}^2$, where k_n, k_{nn}, and k_{bb} are the spring constants for the NN, NNN, and BB springs respectively, and S_{ij} are the components of the strain tensor. It includes both the microscopic strain energy due to the bond distortion in the NWs and the macroscopic strain energy associated with the lattice mismatch between the NWs and the substrate. E_{s} is the NW surface energy, which is considered here as the bond-breaking energy at the surface without consideration of surface reconstruction. The bond-counting model naturally takes into account the dependence of surface energy on surfaces orientation with different surface atom coordination. Also, it qualitatively reproduces the effect of surface segregation, due to both surface

dangling bond energy and strain energy, as shown in our previous simulations of SiGe and InGaN islands[15,16]. However, in the present simulation of kinetic composition of NWs, only local equilibrium is assumed to be established in the top surface layer of growth front, i.e. no intermixing with the subsurface layers, so that no surface segregation is expected.

The entropy is evaluated by a regular-solution-shell-model[15]. $S = -k\sum_{\text{Lattice } i=1}^{N} S_i = -k\sum_{\text{Lattice } i=1}^{N}\left\{\frac{1}{n}\int_V \sum_{\text{Shell } j=1}^{n}\left[x_{ij}\ln\left(x_{ij}\right)+\left(1-x_{ij}\right)\ln\left(1-x_{ij}\right)\right]\right\}$, where k is the Boltzmann constant. The local concentration x_{ij} (i.e., molar fraction) of a component at a given lattice site i is calculated within the lattice shell j centered at i and the local entropy S_i is obtained by averaging all the shells centered at i, as illustrated in Fig. 2. Convergence tests have been done with respect to the sizes and number of the shells, for which the entropy is found converged quickly upon the increasing size and number of the shells. The elastic constants are set to represent specific alloy systems according to the experimental values of $In_xGa_{1-x}N$ and our model produces the interaction parameters of mixing $\Omega_{\text{InGaN}} = -5.16\times10^{-4}x + 0.36$ eV/cation , which agree well with previous first principles[24] and valence force field results[25].

As a qualitative study of the general mechanisms of spontaneous core-shell formation in NWs, we used a two-dimensional (2D) atomistic strain model on a square lattice to calculate the Gibbs free energy of coherently strained alloy NWs on a substrate, as illustrated in Fig. 2 (The number of lattice points in Fig. 2 is schematically reduced for clarity). Qualitatively the same results are obtained by the 2D and the 3D simulations as shown in the previous work[15]. As shown for QDs,[15,16] this 2D generic model should capture the essential physics of the phase segregation of alloy structures, because alloys with different lattice structures and materials are expected to behave in qualitatively the same manner. Without losing generality, we have chosen results of $In_{0.3}Ga_{0.7}N$ NWs as examples because phase separation in InGaN has profound practical implications for LEDs, lasers and solar cells[26].

A Monte Carlo method[27] combined with force-balance approach is used to minimize the total free energy and find the optimal alloy composition profile at typical growth temperature 900 K. The quantitative CPs are slightly changed with different temperatures but the qualitative composition patterns will not be altered. A schematic flow chart of our simulation is shown in Fig. 3. At each time step of atom exchange, the strain energy of the resulting alloy configuration is minimized by the force-balance equation, $\partial E / \partial \mathbf{u}(\mathbf{i}) = 0$, where $\mathbf{u}$ is the displacement, to optimize the atomic structure of the given distribution. The energy is considered converged when the energy differences between the current step and the 10 preceding steps are all less than 0.1% of current energy. If all the atoms in the NW are allowed to exchange their positions, the global equilibrium composition profile is established; if the exchanges are confined in the surface regions of the NW, local equilibrium is reached only in the surface regions.

We have performed tests on InGaN NWs ranging from 10 nm to 60 nm in base size, with lattices containing up to a few tens of thousands of lattice points. For NWs with fixed alloy composition, our results are found to be size independent as long as the local equilibrium is established in the growth front (high temperature and low deposition rate). For presentation purpose, we will show the results of 30 nm NW as examples. Interdiffusion between the NW and substrate is excluded for simplicity. Since the atom exchange only happens in the surface layer of growth front as suggested by the experiments[28,29], the interdiffusion between wire and substrate is not expected to be significant for the kinetic growth compositions. As for the equilibrium composition, the result is only very slightly affected because the concentrations of the strained components in lower part of the NWs are very low.

III. RESULTS AND DISCUSSION

First, we simulated the equilibrium CPs of strained InGaN NWs, as shown in Fig. 4. To reach the equilibrium CP, all atoms in the NW are allowed to exchange positions to minimize the total energy using the MC algorithm. Figure 4 shows the equilibrium In concentration profile in an $In_{0.3}Ga_{0.7}N$ NW. Because of the large height/width aspect ratio, the top regions of the NW are fully relaxed, while the base regions are constrained to be coherent with the substrate, with the In concentration decreasing

continuously from the top to the base. Nearly all In atoms (the strained component) segregate towards the top surface with a slight enrichment in the two top corners and most of Ga atoms (the unstrained component) are incorporated in the base. Strain is predominantly responsible for the phase separation and in addition, the large positive enthalpy of mixing[26] and the existence of a miscibility gap[30] further favor phase segregation. The local maximum In concentration at the top surface corresponds to the thermodynamic equilibrium concentration at the given temperature and precursor concentration[26].

Next, we describe the inclusion of kinetic factors that produce non-equilibrium CPs, in particular the kinetically controlled phase separation processes that will lead to spontaneous core-shell nanostructure formation in InGaN NWs. Although the thermodynamic equilibrium distribution may be reached in very small nanostructures grown at relatively high temperatures, where diffusion allows redistribution of the alloy components within the entire nanostructures, it is generally not expected for larger nanostructures. This is because bulk diffusion is negligible at typical growth temperatures, having much too high an energy barrier, such as ~3.4 eV for interdiffusion of In and Ga in InGaN[19]. However, the barriers are greatly reduced at surfaces. For example, diffusion activation energies of ~0.4 eV for Ga surface diffusion on GaN(0001)[20]. This allows local equilibrium CPs to be established in the surface regions during epitaxial growth. Consequently, the kinetic growth mode, which dictates the surface mass transport and alloy mixing via surface diffusion at the growth front, becomes a key factor in determining the kinetically limited CP. In order to reveal the underlying relationship between the kinetically controlled core-shell structure of the epitaxial strained alloy NWs and the growth mode, we investigated the effects of two typical growth modes, LG versus FG, on the spontaneous formation of core-shell structures in InGaN NWs.

Figure 5 illustrates the typical VLS growth process of a NW. During VLS growth, the melted catalyst can rapidly adsorb alloy from vapor to form liquid eutectic. The NW growth then happens at the liquid–solid interface and its size is thus limited by the size of the liquid droplet. In the LG mode (Fig. 5b), the NW growth front proceeds in the substrate surface normal direction, with successive nucleation and growth of new surface layers, each on top of the previously completed surface layer. In the FG mode

(Fig. 5c), the NW growth front proceeds in the NW surface facet normal direction, with successive nucleation and growth of new facets on top of the previously completed NW facets.

As noticed in the recent experiments, the interfaces between two sections with different materials in the NWs grown by VLS method are atomically sharp[28,29], which suggests that the effective diffusion only occurs in the surface layer. Thus we assumed that in both modes of growth, the local equilibrium composition is reached only in the outmost surface (or facet) layer and the equilibrated surface composition is subsequently frozen upon the growth of the following layer. Such kinetically limited growth leads to the spontaneous formation of core-shell structured NWs (Fig. 5d and e). The LG yields structures with cores rich in the unstrained component (Fig. 5d and Fig. 5f solid line, $x_{GaN} \sim 1.0$ in the core), while the FG mode yields structures with cores rich in the strained component (Fig. 5e, and Fig. 5f dashed line, $x_{InN} \sim 1.0$ in the core). These growth-mode-controlled alloy CPs are distinctively different from the equilibrium CPs shown in Fig. 4.

The above results can be qualitatively understood in terms of different strain relaxation mechanisms associated with the different growth modes. In the LG mode, the growth front is flat. When the atoms are equilibrated within this flat layer, strain relaxation results in a "lateral" phase separation with the strained component (InN) segregating to the outside (i.e., the most relaxed region) and the unstrained component (GaN) to the center of the surface layer. In contrast, in the FG mode, the growth front is inclined at a fixed angle with the substrate surface normal direction. When the atoms are equilibrated within this inclined facet layer, strain relaxation results in a "vertical" phase separation with InN segregating to the top (i.e., the most relaxed region) and GaN to the bottom of the facet. The segregated surface compositions are successively frozen in as the growth proceeds. Such lateral versus vertical segregation patterns in the LG versus FG give rise to the different core-shell structures of NWs. In the VLS growth of NWs, the growth fronts in both growth modes have a constant size, determined by the size of the liquid eutectic, so that the amount of In atoms segregated with the growth front remains the same, leading to a vertical columnar core-shell structure with constant width.

Based on our literature search, we found all the existing self-assembled core-shell alloy NWs grown by VLS have a core rich in the unstrained (or less strained) component[9-12], indicating that they are all grown via the LG mode as shown in Fig. 5d. This is consistent with some recent experimental studies that suggested also the LG growth mechanism[28,29]. On the other hand, however, different orientation of facets at the solid-liquid interfaces have been seen in the growth of Si NWs (Fig. 5e)[31], confirming the feasibility of faceted growth for alloy NWs. Thus, our findings suggest a possible route towards controlling the core-shell CPs in alloy NWs by altering growth mode, such as adopting those techniques for growing Si NWs[31].

The definition of "strained" or "unstrained" component in a NW is based on the epitaxial relation between the NW and substrate, which may be altered by changing the substrate. Thus, we have studied the influence of the substrate. Figure 6 shows the calculated CPs of the InGaN strained alloy NWs grown by the LG mode (Fig. 6a and Fig. 6c solid line) versus the FG mode (Fig. 6b and Fig. 6c dashed line) on the InN substrate. Compared with the results on the GaN substrate shown in Fig. 5, almost exactly opposite core-shell CPs are obtained. This is expected since the corresponding "unstrained component" changes from GaN to InN as the substrate changes from GaN to InN. We point out that although InN is currently an unavailable substrate, one can still choose a substrate with similar crystal structure and lattice constant of InN, such as $(Mn,Zn)Fe_2O_4$ (111)[32] to achieve the same or similar results. We note that the macroscopic misfit strain between the NWs and the substrate plays an essential role in achieving the phase separation. Without the macroscopic strain, i.e, if the NW and the substrate are lattice matched, uniformly distributed CPs of $In_{0.3}Ga_{0.7}N$ NWs will grow irrespective to growth mode.

IV. CONCLUSIONS

In conclusion, our simulation results and findings suggest a possible route towards controlling the core-shell CPs of NWs by controlling the growth mode, through changing growth parameters such as temperature, deposition rate, pressure and precursor, and/or surface conditions such as adding surfactant effects[33,34]. In particular, we suggest some tricks for growing single-element Si NWs[31] with different

faceted orientations of solid-liquid interface might be borrowed to grow alloy NWs to achieve different growth modes. Furthermore, substrate engineering can be used to change the magnitude and sign of misfit strain between the NW and the substrate to tune and even reverse the core-shell CPs of alloy NWs. These strategies will be generally applicable to the development of strained alloy nanostructures for applications in photonic and electronic devices.

ACKNOWLEDGMENTS

This work was supported by the Department of Energy, Basic Energy Sciences division (Grant No. DE-FG02-04E46148) and the Cao Group. We thank the Center for High Performance Computing at University of Utah and NERSC for providing the computing resources. We also thank Oliver Schmidt and Anil Virkar for helpful discussions.

FIG. CAPTIONS

Fig. 1. Schematic illustration of the 2D atomistic strain model on a square lattice. k_n, k_{nn}, and k_{bb} are the spring constants for the NN, NNN, and BB springs, respectively.

Fig. 2. (Color online) Schematic illustration of simulation frame work and the regular-solution-shell model. The simulations are performed in a 2D model using a square lattice, as indicated by a reduced number of lattice points for clarity. Zero boundary condition (ZBC) at the bottom of the substrate and periodic boundary conditions (PBC) in the lateral direction are used.

Fig. 3. (Color online) Flow chart of detailed Monte Carlo process used in our simulations.

Fig. 4. (Color online) Thermodynamic equilibrium CPs of a $In_{0.3}Ga_{0.7}N$ NW grown on GaN substrate. The colored arrow shows the segregation directions of InN (red/gray)/GaN (yellow/white). The simulated InN concentrations are color-coded in a contour plot, as scaled by color bars.

Fig. 5. (Color online) Kinetically controlled InN core-shell CPs of heteroepitaxial $In_{0.3}Ga_{0.7}N$ NWs grown on GaN substrates by different growth modes. (a) Schematic illustration of the typical VLS growth process of a strained NW. (b) Schematic illustration of the LG mode for a NW. (c) The FG mode for a NW. (d) Contour plot of CP of a NW with a columnar GaN-rich core, resulting from the LG mode. (e) Contour plot of CP of a NW with a columnar InN-rich core, resulting from the FG mode. (f) The averaged InN concentration along the diameter of the NWs. The colored arrow shows the InN (red/gray)/GaN (yellow/white) segregation directions and the color bar marks the InN concentration.

Fig. 6. (Color online) Kinetically controlled InN core-shell CPs for heteroepitaxial $In_{0.3}Ga_{0.7}N$ NWs grown on InN substrates by different growth modes. (a) Contour plot of CP of a NW with a columnar InN-rich core, resulting from the LG mode. (b) Contour plot of CP of a NW with a columnar GaN-rich core, resulting from the FG mode. (c) The averaged InN concentration along the diameter of the NWs.

The colored arrow shows the InN (red/gray)/GaN (yellow/white) segregation directions and the color bar marks the InN concentration.

REFERENCES

1. X. Duan, Y. Huang, Y. Cui, J. Wang and C. M. Lieber, Nature **409**, 66 (2001).

2. Z. Zhong, F. Qian, D. Wang and C. M. Lieber, Nano Lett. **3**, 343 (2003).

3. M. H. Huang, S. Mao, H. Feick, H. Yan, Y. Wu, H. Kind, E. Weber, R. Russo and P. Yang, Science **292**, 1897 (2001).

4. X. Duan, Y. Huang, R. Agarwal and C. M. Lieber, Nature **421**, 241 (2003).

5. B. Tian, X. L. Zheng, T. J. Kempa, Y. Fang, N. F. Yu, G. H. Yu, J. L. Huang and C. M. Lieber, Nature **449**, 885 (2007).

6. M. S. Gudiksen, L. J. Lauhon, J. F. Wang, D. C. Smith and C. M. Lieber, Nature **415**, 617 (2002).

7. L. J. Lauhon, M. S. Gudiksen, D. Wang and C. M. Lieber, Nature **420**, 57 (2002).

8. N. Sköld, L. S. Karlsson, M. W. Larsson, M. E. Pistol, W. Seifert, J. Trägårdh and L. Samuelson, Nano Lett. **5**, 1943 (2005).

9. P. K. Mohseni, A. D. Rodrigues, J. C. Galzerani, Y. A. Pusep, R. R. LaPierre, J. Appl. Phys. **106**, 124306 (2009).

10. X. M. Cai, Y. H. Leung, K. Y. Cheung, K. H. Tam, A. B. Djurišić, M. H. Xie, H. Y. Chen and S. Gwo, Nanotechnology **17**, 2330 (2006).

11. C. Chen, S. Shehata, C. Fradin, R. LaPierre, C. Couteau and G. Weihs, Nano Lett. **7**, 2584 (2007).

12. H. J. Choi, J. C. Johnson, R. He, S. K. Lee, F. Kim, P. Pauzauskie, J. Goldberger, R. J. Saykally and P. Yang, J. Phys. Chem. B **107**, 8721 (2003).

13. P. Venezuela, J. Tersoff, J. A. Floro, E. Chason, D. M. Follstaedt, F. Liu and M. G. Lagally, Nature **397**, 678 (1999).

14. L. Bai, J. Tersoff and F. Liu, Phys. Rev. Lett. **92**, 225503 (2004).

15. X. B. Niu, G. B. Stringfellow and F. Liu, Phys. Rev. Lett. **107**, 076101 (2011).

16. X. B. Niu, G. B. Stringfellow and F. Liu, Appl. Phys. Lett. **99**, 213102 (2011).

17. T. Kuykendall, P. Ulrich, S. Aloni and P. Yang, Nature Mater. **6**, 951 (2007).

18. W. Guo, M. Zhang, A. Banerjee and P. Bhattacharya, Nano Lett. **10**, 3355 (2010).

19. C. C. Chuo, C. M. Lee and J. I. Chyi, Appl. Phys. Lett. **78**, 314 (2001).

20. T. K. Zywietz, J. Neugebauer and M. Scheffler, Appl. Phys. Lett. **73**, 487 (1998).

21. J. M. Reich, X. B. Niu, Y. J. Lee, R. E. Caflisch and C. Ratsch, Phys. Rev. B **79**, 073405 (2009).

22. A. C. Schindler, M. F. Gyure, G. D. Simms, D. D. Vvedensky, R. E. Caflisch, C. Connell and E. Luo, Phys. Rev. B **67**, 075316 (2003).

23. C. Connell, R. E. Caflisch, E. Luo and G. Simms, J. Comput. Appl. Math. **196**, 368 (2006).

24. D. L. A. Camacho, R. H. Hopper, G. M. Lin, B. S. Myers, M. Van Schlifgaarde, A. Sher and A. B. Chen, J. Cryst. Growth **178**, 8 (1997).

25. T. Saito and Y. Arakawa, Phys. Rev. B **60**, 1701 (1999).

26. G. B. Stringfellow, J. Cryst. Growth **312**, 735 (2010).

27. N. Metropolis, A. W. Rosenbluth, M. N. Rosenbluth, A. H. Teller and E. Teller, J. Chem. Phys. **21**, 1087 (1953).

28. J. Johansson, L. S. Karlsson, C. P. T. Svensson, T. Mårtensson, B. A. Wacaser, K. Deppert, L. Samuelson and W. Seifert, Nature Mater. **5**, 574 (2006).

29. M. T. Björk, B. J. Ohlsson, T. Sass, A. I. Persson, C. Thelander, M. H. Magnusson, K. Deppert, L. R. Wallenberg and L. Samuelson, Appl. Phys. Lett. **80**, 1058 (2002).

30. I. Ho and G. B. Stringfellow, Appl. Phys. Lett. **69**, 2701 (1996).

31. Y. Wu, Y. Cui, L. Huynh, C. J. Barrelet, D. C. Bell and C. M. Lieber, Nano Lett. **4**, 433 (2004).

32. J. Ohta, K. Mitamura, A. Kobayashi, T. Honke, H. Fujioka and M. Oshima, **137**, 208 (2006).

33. E. Rudkevich, F. Liu, D. E. Savage, T. F. Kuech, L. McCaughan and M. G. Lagally, Phys. Rev. Lett. **81**, 3467 (1998).

34. J. Y. Zhu, F. Liu and G. B. Stringfellow, Phys. Rev. Lett. **101**, 196103 (2008).

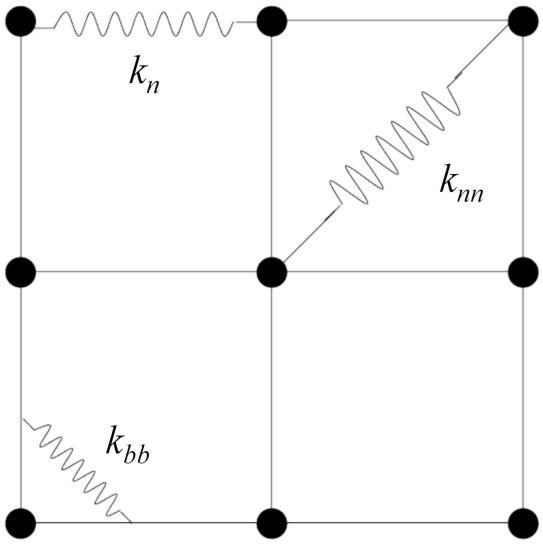

Figure 1 BNR1145B 02APR2012

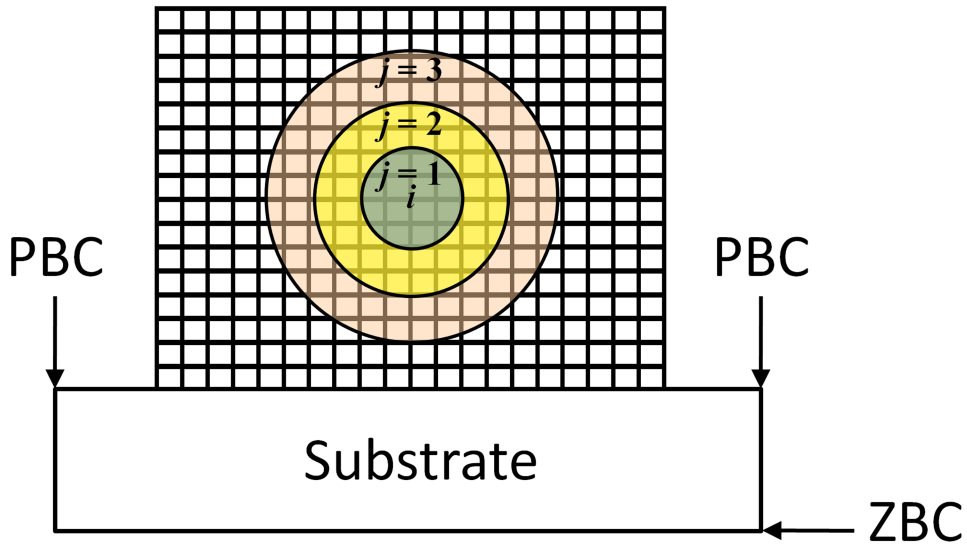

Figure 2 BNR1145B 02APR2012

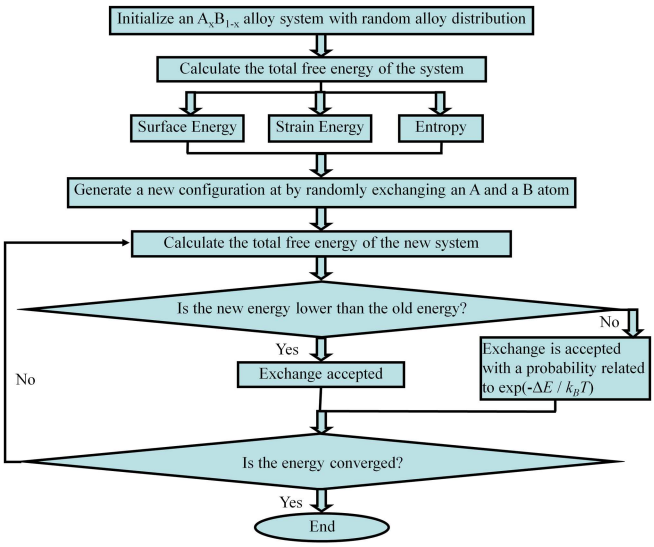

Figure 3 BNR1145B 02APR2012

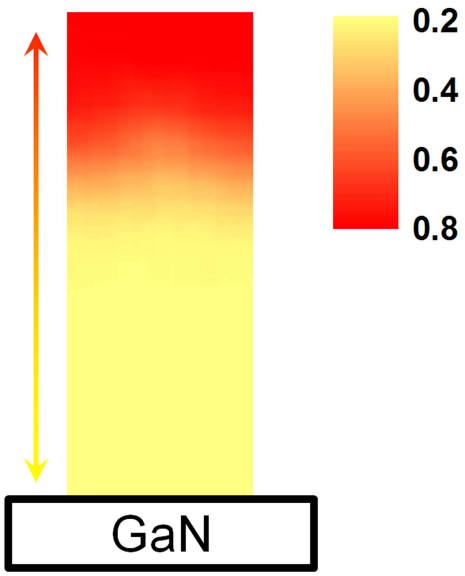

Figure 4 BNR1145B 02APR2012

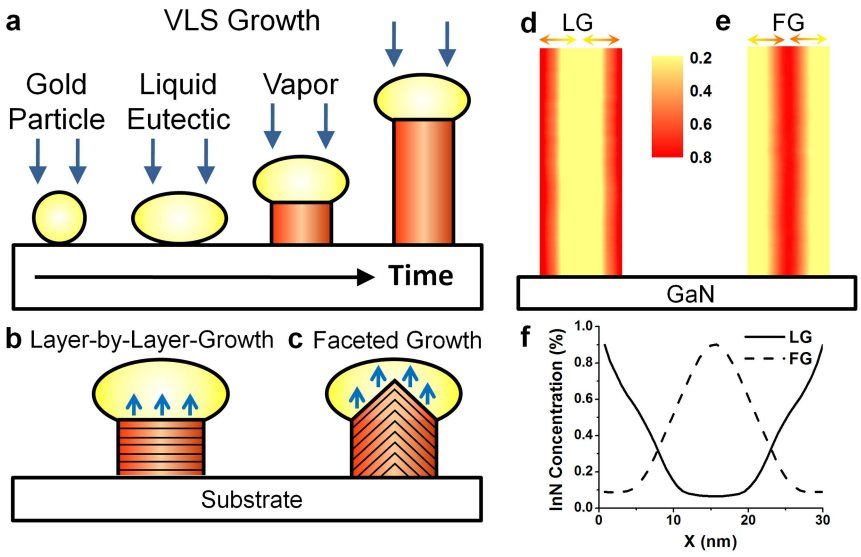

Figure 5 BNR1145B 02APR2012

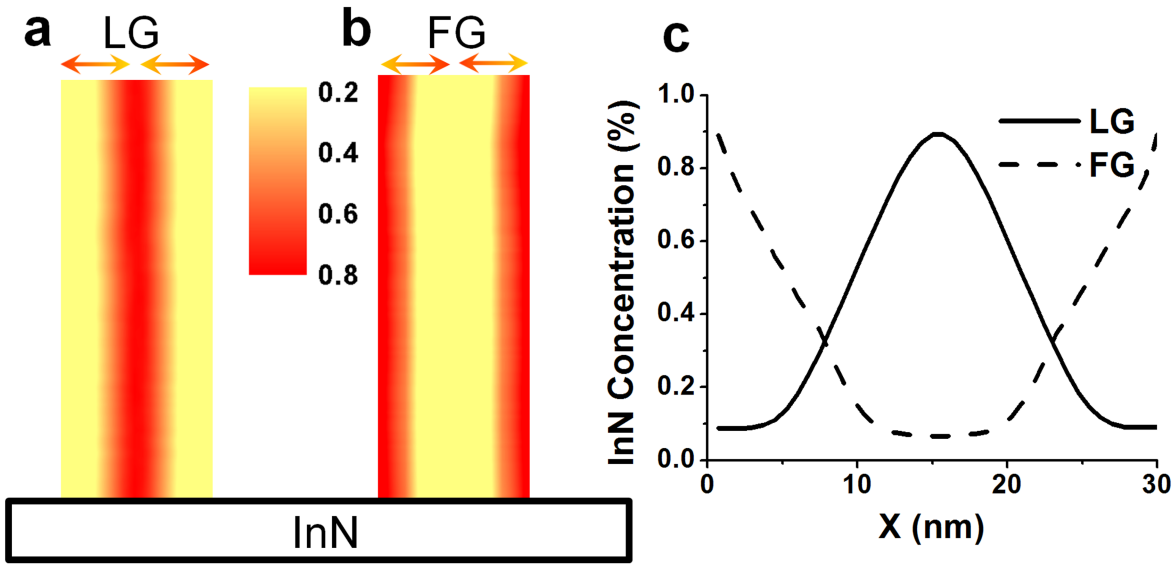

Figure 6 BNR1145B 02APR2012